Inorganic Chemistry

pubs.acs.org/IC

Article

Origin of Weak Magnetic Coupling in a Dimanganese(II) Complex Bridged by the Tetrathiafulvalene-Tetrathiolate Radical

Chen-Yu Lien, Jan-Niklas Boyn, Sophie W. Anferov, David A. Mazziotti, and John S. Anderson*

Cite This: *Inorg. Chem.* 2023, 62, 19488−19497

Read Online

ACCESS | Metrics & More | Article Recommendations | Supporting Information

ABSTRACT: Magnetic exchange coupling (J) between different spin centers plays a crucial role in molecule-based magnetic materials. Direct exchange coupling between an organic radical and a metal is frequently stronger than superexchange through diamagnetic ligands, and the strategy of using organic radicals to engender desirable magnetic properties has been an area of active investigation. Despite significant advances and exciting bulk properties, the magnitude of J for radical linkers bridging paramagnetic centers is still difficult to rationally predict. It is thus important to elucidate the features of organic radicals that govern this parameter. Here, we measure J for the tetrathiafulvalene-tetrathiolate radical ($TTFtt^{3-\bullet}$) in a dinuclear Mn(II) complex. Magnetometry studies show that the antiferromagnetic coupling in this complex is much weaker than that in related Mn(II)−radical compounds, in contrast to what might be expected for the S-based chelating donor atoms of TTFtt. Experimental and computational analyses suggest that this small J coupling may be attributed to poor overlap between Mn- and TTFtt-based magnetic orbitals coupled with insignificant spin density on the coordinating S-atoms. These factors override any expected increase in J from the comparatively strong S-donors. This work elucidates the magnetic coupling properties of the $TTFtt^{3-\bullet}$ radical for the first time and also demonstrates how multiple competing factors must be considered in rationally designing organic radical ligands for molecular-based magnetic compounds.

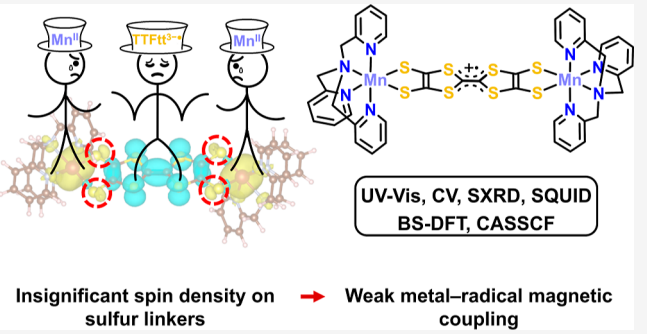

INTRODUCTION

Molecule-based magnetic compounds, including discrete molecules and extended frameworks, have attracted significant attention in recent decades.[1−10] The tunability of molecular systems opens up possibilities for switchable magnetic properties via redox control,[11−14] irradiation,[15−17] or solvation/desolvation processes.[18−21] Furthermore, bottom-up synthetic approaches allow for systematic studies of structure−property relationships.[22−24] By controlling supramolecular interactions and combining the properties of different building blocks, stimuli-responsive or multifunctional magnetic materials have also been developed.[25−31]

A central physical quantity in molecular magnetism is the exchange coupling constant between different spin centers, J. The value of J is correlated to the spin ground state, which intimately affects properties such as bulk ordering temperatures (T_c),[32−34] magnetization relaxation barriers,[2,10] and even suppression of undesired quantum tunneling of magnetization.[35−37] Classical examples of molecule-based magnetic materials typically rely upon superexchange coupling mediated by diamagnetic linkers between paramagnetic centers.[1,38,39] Superexchange coupling strength decreases drastically as the length of the bridging ligand increases, mandating short distances between spin centers and thus significantly limiting the design space of new materials.[40] For instance, common structural motifs include oxo-bridged metal clusters and cyano-bridged Prussian blue analogues,[8,41−46] although other ligands such as azide, N-heterocycles, formate, and other carboxylate derivatives have been adopted as well.[1,38,47]

To access chemically more diverse structures while maintaining strong exchange coupling, one promising approach is using organic radical bridging ligands.[1,2,48,49] Radical-mediated coupling is usually stronger than the aforementioned superexchange interactions, particularly over longer diamagnetic bridges (i.e., >3 atoms). Over the past few decades, moieties including nitroxyl, verdazyl, and semiquinoid radicals have been incorporated into both discrete complexes and extended frameworks.[1,2] Excitingly, this strategy enables high magnitudes of J ($\sim 10^2$ to 10^3 cm^{-1}) in some compounds,[50,51] demonstrating the promise of this approach. Still, despite these exciting advances, unified design principles for mediating strong coupling with radical ligands remain

Received: July 24, 2023
Revised: October 25, 2023
Accepted: October 30, 2023
Published: November 15, 2023

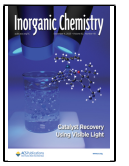

https://doi.org/10.1021/acs.inorgchem.3c02534
Inorg. Chem. 2023, 62, 19488−19497

elusive. The relative importance of trade-offs between factors such as spin−spin distance, spin density and localization, and/or metal−ligand energetic matching in specific systems is still not well understood.

As an illustrative set of compounds, several examples of di-Mn(II) complexes with bridging organic radical ligands have been reported (Figure 1).[52−55] Mn(II) is an attractive ion for

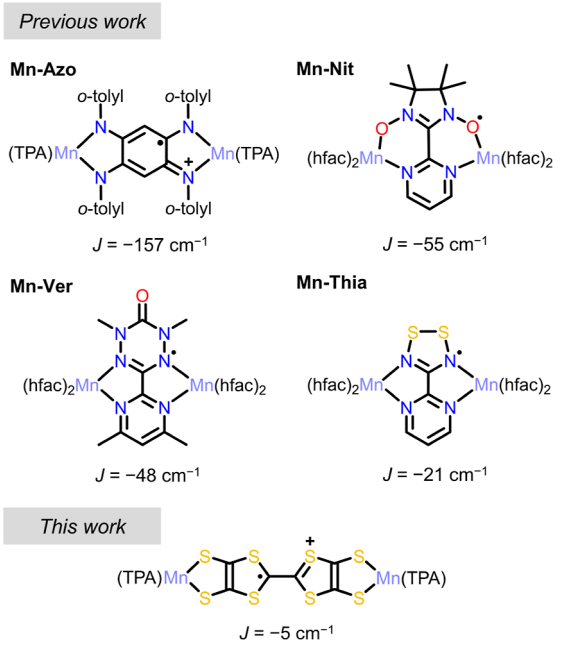

Figure 1. Radical-bridged dinuclear Mn(II) complexes and corresponding experimental magnetic coupling constants (J) in the previous and this work. TPA = tris(2-pyridylmethyl) amine, hfac = hexafluoroacetylacetonate.

these studies due to the absence of convoluting spin−orbit coupling or spin-crossover effects. Several examples of these complexes reveal a wide range of direct exchange coupling magnitudes: the largest $J_{\text{Metal−Radical}}$ is observed for an azophenine-bridged dinuclear Mn(II) complex, and this value is 1 order of magnitude larger than that of a dithiadiazolyl-bridged analogue.[52,53] Notably, the Mn···Mn distance is larger in the azophenine case, but this example still shows a larger coupling. An important factor in this direct exchange is the identity of the binding atom of the linker. For instance, in a series of quinoid-bridged Cr(III) complexes with nitrogen, oxygen, or sulfur linkers, the magnitude of J trends as nitrogen > sulfur > oxygen.[52,56] However, comparison of the coupling of nitronyl nitroxide (O-bound) and verdazyl (N-bound) Mn(II) complexes in Figure 1 breaks with this trend. Therefore, the underlying design principles to engender strong magnetic coupling are not well-defined, which motivates continued efforts in this area.

Recently, we have been studying dinuclear complexes and coordination polymers based on redox-active tetrathiafulvalene-2,3,6,7-tetrathiolate ($TTFtt^{n-}$, n = 4, 3, and 2) ligands.[57−61] These compounds display a variety of properties including high electrical conductivity,[61] near-infrared photoluminescence,[59] and spin transitions.[58] However, the magnetic properties of complexes with a monoradical TTFtt linker, namely, with a formal charge of 3−, have not been thoroughly investigated.[57] We were specifically curious about how strongly this linker would mediate exchange coupling as it has been shown that sulfur-based radical linkers facilitate stronger magnetic coupling than oxygen-based congeners.[56] We therefore studied the magnetic properties of complexes containing sulfur-based $TTFtt^{3-}$ and paramagnetic metals.

Herein, we report a dinuclear Mn(II) complex $\{[(TPA)Mn]_2TTFtt\}\{BAr^F{}_4\}$ (**1**) (TPA = tris(2-pyridylmethyl) amine, $BAr^F{}_4$ = tetrakis[3,5-bis(trifluoromethyl)-phenyl]borate), which features paramagnetic metals bridged by the $TTFtt^{3-\bullet}$ radical, enabling examination of how the TTFtt linker mediates exchange coupling. In contrast with previous studies that suggest that S-based linkers should mediate comparatively stronger exchange coupling, we measure only weak antiferromagnetic coupling between Mn(II) and $TTFtt^{3-\bullet}$. Broken-symmetry density functional theory (BS-DFT) and complete active space self-consistent field (CASSCF) calculations suggest that very little spin density is localized on the coordinating-S of $TTFtt^{3-\bullet}$,[62,63] which explains the small magnitude of J. This distinct electronic structure of $TTFtt^{3-\bullet}$ provides guidance on the design of TTFtt-derived materials and underscores how multiple properties must be considered in the design of radical bridging ligands for molecular magnetic compounds.

RESULTS AND DISCUSSION

Synthesis and Characterization. The synthesis of complex **1** (Scheme 1) was based on a related procedure for an Fe(II) analogue with slight modifications.[58] The proligand $TTFtt(CH_2CH_2CN)_4$ was deprotected with a base in tetrahydrofuran (THF) and then mixed with $(TPA)MnCl_2$

Scheme 1. Synthesis of Complex 1

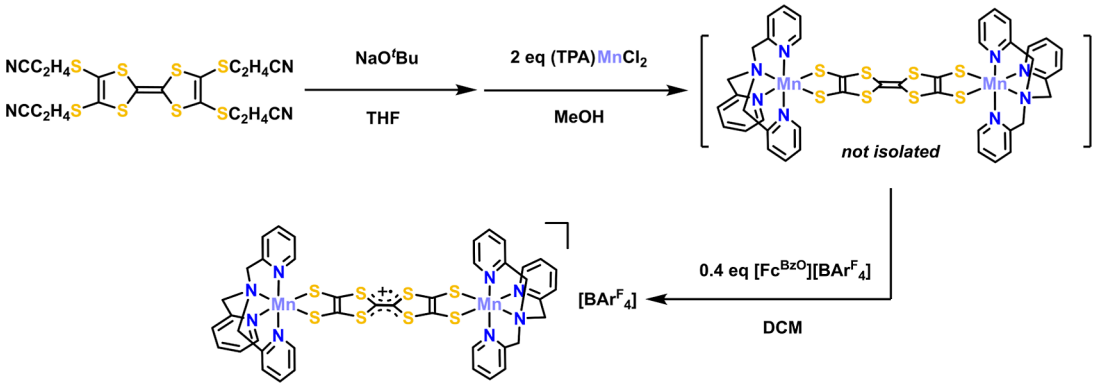

https://doi.org/10.1021/acs.inorgchem.3c02534
Inorg. Chem. 2023, 62, 19488−19497

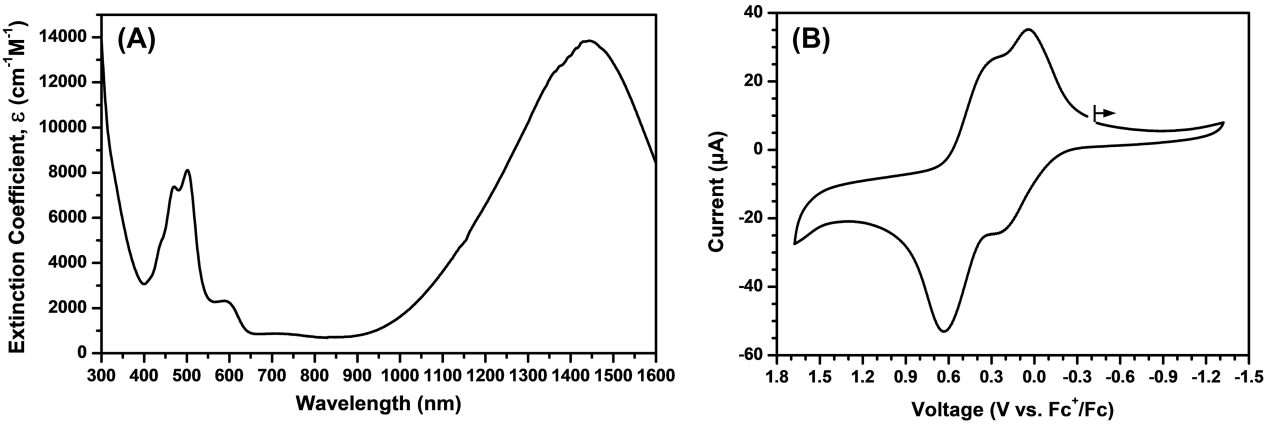

Figure 2. (a) UV−vis−NIR spectrum and (b) cyclic voltammogram of **1** in DCM. In (b), scan rate: 0.1 V/s and electrolyte: 0.1 M [^{n}Bu$_4$N][PF$_6$].

in methanol to afford a red-orange solid. This solid is poorly soluble in most organic solvents and thus is difficult to characterize, but it is presumably a dinuclear Mn complex bridged by TTFtt^{4-}. We directly oxidized this solid without further purification with [Fc^{BzO}][BAr$^{F}_4$] (Fc^{BzO} = benzoyl ferrocenium) in dichloromethane (DCM) and were able to crystallize complex **1** from this mixture in a moderate yield (57%). The UV−vis−NIR spectrum of **1** (Figure 2A) shows relatively sharp peaks at 450−500 nm and a broad feature in the NIR region with a maximum at 1444 nm. Both of these features are characteristic of previous complexes with TTFtt$^{3-\bullet}$ linkers.[57] The cyclic voltammogram of **1** (Figure 2B) shows two quasi-reversible features at 0.14 and 0.48 V vs Fc^{+}/Fc, which are assigned as the TTFtt 4−/3−• and 3−•/2− couples, respectively. Similar redox events are observed for related TTFtt-bridged dinuclear complexes, though we note that complex **1** is comparatively more oxidizing.[57−59]

Solid-State Structures. Single crystals of complex **1** were grown via petroleum ether vapor diffusion into a DCM/chlorobenzene solution. There are two molecules per asymmetric unit with only minor structural differences (Figure 3). The Mn centers adopt a distorted octahedral geometry,

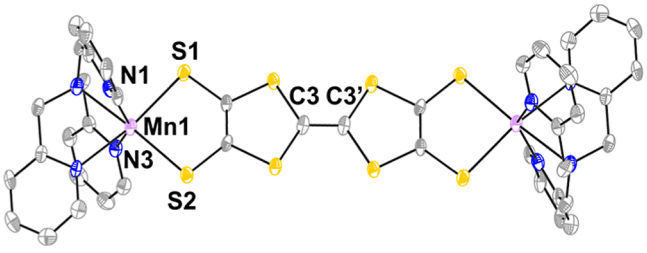

Figure 3. Single crystal structure of **1**. Selected average bond lengths: Mn1−S1 2.476(1) Å, Mn1−S2 2.543(1) Å, and C3−C3′ 1.37(1) Å. Selected bond angle: N1−Mn1−N3 145.1(1)°. Only one of two asymmetric TTFtt units is shown. Hydrogen atoms and chlorobenzene molecules have been omitted for clarity, and ellipsoids are shown at 50% probability. C: gray, N: blue, S: yellow, and Mn: purple.

where N1−Mn1−N3 is ∼145°. The distortion is likely due to the chelate rings of the TPA ligand, and similar distortions are observed in another dinuclear Mn complex with TPA capping ligands.[52] The Mn−S bond lengths range from 2.470(2) to 2.548(2) Å, which are similar to those reported in other Mn(II)−dithiolene structures.[64−66] The central C−C bond lengths of the bridging TTFtt moiety are 1.36(2) and 1.37(2) Å, which are also similar to the values in Sn(IV) and Ni(II) complexes bridged by TTFtt$^{3-\bullet}$.[57] TTFtt $\pi-\pi$ stacking interactions are not observed in **1**, contrary to previously reported square planar Ni(II) complexes,[57] which may reasonably be attributed to the steric effect from the chelating TPA ligands. The shortest intermolecular contacts are 2.7−2.8 Å and occur between peripheral pyridine rings and between the TPA methylene C−H and the carbon on TTFtt (Figure S1A). These interactions link the cationic TTFtt complexes in a 2D fashion, with the interlayer space occupied by BAr$^{F}_4{}^{-}$ counteranions and solvated chlorobenzene molecules (Figure S1B).

Magnetometry. We measured the magnetic susceptibility of complex **1** in the solid state between 1.8 and 300 K at 0.1 and 1 T (Figures 4 and S4). The χT value of **1** is 9.0 cm^3 K/mol at 300 K, which is close to the theoretical value of 9.13 cm^3 K/mol for two uncoupled S = 5/2 Mn(II) centers and an S = 1/2 TTFtt$^{3-\bullet}$ ligand. The solution-state magnetic moment, as measured by Evans' method, also provides a similar value of 8.9 cm^3 K/mol (Figure S3). The solid-state χT value decreases slightly upon cooling before increasing below 40 K to a maximum of 10.3 cm^3 K/mol at ∼6 K and then dropping with additional cooling. This behavior is similar to other dinuclear radical-bridged complexes and suggests net ferrimagnetic coupling between the two Mn(II) centers and the TTFtt$^{3-\bullet}$

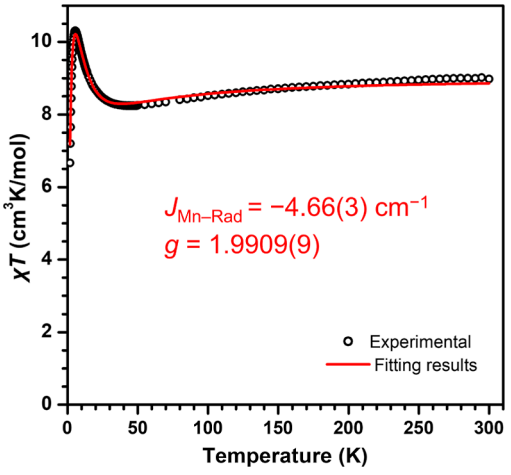

Figure 4. Variable-temperature magnetic susceptibility data of **1** in the solid state measured at 1 T.

https://doi.org/10.1021/acs.inorgchem.3c02534
Inorg. Chem. 2023, 62, 19488−19497

Table 1. Selected Experimental and Calculated Parameters of 1 and Other Mn(II) Complexes

compound	exp. J (cm^{-1})	computational J (cm^{-1})			average of normalized Mn−linker lengths in the crystal structure	corresponding orbital overlap integral[b]	sum of spin densities on coordinating atoms[b]	
		DFT	CASSCF	NEVPT2			DFT	CASSCF
Mn-Azo	−157	−153	−49	−80	0.927[a]	0.348	0.549	0.195
Mn-Nit	−55	−162	−56	−80	0.980	0.313	0.608	0.563
Mn-Ver	−48	−35	−14	−14	0.992	0.167	0.682	0.493
Mn-Thia	−21	−25	−9	−13	1.00	0.144	0.514	0.311
1	−5	−10	−2	−5	0.943	0.107	0.037	0.031

[a]The single crystal of **Mn-Azo** was not reported. Raw bond lengths used for this analysis were adopted from an analogue with a more oxidized ligand. See Table S2 for details. [b]Based on DFT-optimized structures in the $S = 9/2$ ground state.

linker.[22,52,54,67] We fit the magnetic data with the Hamiltonian $\hat{H} = -2J_{Mn-Rad}[(\hat{S}_{Mn1} + \hat{S}_{Mn2})\cdot\hat{S}_{Rad}]$ using the program PHI.[68] The fitting results suggest weak antiferromagnetic coupling between the Mn(II) centers and $TTFtt^{3-\bullet}$ with $J_{Mn-Rad} = -4.66(3)$ cm^{-1} [$g = 1.9909(9)$]. The precise value of J_{Mn-Rad} is sensitive to the fit range and other parameters, but in all cases, $|J_{Mn-Rad}|$ is < 10 cm^{-1} (see Figure S4 for alternative fits). Interestingly, the magnitude of J_{Mn-Rad} in **1** is notably smaller than those in other Mn(II)−radical species. For example, the dinuclear Mn(II) complexes with verdazyl and nitronyl nitroxide ligands shown in Figure 1 have J_{Mn-Rad} of −48 and −55 cm^{-1}, respectively.[54,55] Mononuclear Mn(II) complexes with the same ligands also provide similar magnitudes of J_{Mn-Rad}.[69,70] The aforementioned dinuclear complex containing an azophenine radical shows much stronger coupling with J_{Mn-Rad} of −157 cm^{-1}.[52] The markedly weaker coupling in **1**, despite the presence of putatively more covalent M−S bonds with better overlap, led us to examine the coupling in this complex in more detail.

Magneto−Structural and Computational Analysis. To understand the unexpectedly weak antiferromagnetic coupling in **1**, we performed DFT, CASSCF, and *n*-electron valence state perturbation theory to second-order (NEVPT2) calculations on **1** and the other complexes displayed in Figure 1.[71] Structures were initially optimized at the spin-unrestricted PBE0/def2-SVP level of theory for the $S = 9/2$ state,[72,73] followed by broken-symmetry fragment-guess single point calculations at the PBE0/def2-TZVP level of theory as implemented in Gaussian 16 Rev. A.03.[74] CASSCF and NEVPT2 calculations were performed with the def2-SVP basis set utilizing density fitting for both Coulomb and exchange integrals with the def2/JK auxiliary basis as implemented in ORCA 5.0.3.[75,76] Values for J were obtained using the Yamaguchi formula, $J = \frac{E_{LS} - E_{HS}}{\langle \hat{S}^2_{HS} \rangle - \langle \hat{S}^2_{LS} \rangle}$,[77] and CASSCF and NEVPT2 energies were obtained utilizing state-averaging of $S = 1/2$, $9/2$, and $11/2$ states with equal weights. The computational data are displayed in Tables 1 and S1. For each surveyed complex, the central fragment containing the bridging radical and two Mn(II) centers is mostly superimposable when the DFT-optimized and single-crystal structures are compared (Figure S5). It is worth noting that in **Mn-Ver**, the oxoverdazyl and the pyrimidine are coplanar in the DFT-optimized structure, while they are twisted in the single crystal with a dihedral angle of ∼25°. In terms of coordination geometry, in **Mn-Thia**, Mn(II) is a typical trigonal prism in the single crystal, but DFT predicts that Mn(II) is slightly closer to octahedral as analyzed by the SHAPE program (Table S2).[78] However, the DFT-calculated J values of **Mn-Ver** and **Mn-Thia** do not greatly deviate from experimental values (vide infra).

In accordance with the experimentally observed antiferromagnetic coupling, both DFT and multireference methods predict the $S = 9/2$ state to be the ground state for all surveyed compounds. Values for J obtained with broken-symmetry DFT generally show good agreement with the experiment and yield the correct ordering across the series of compounds, except for **Mn-Nit**, for which the magnitude of J is overestimated significantly. CASSCF, in turn, tends to underestimate the magnitude of J due to the lack of dynamic correlation resolved in the calculation and inclusion of which via NEVPT2 generally increases the magnitude of J to improve agreement with the experiment. We do note that NEVPT2 displays a significant basis set dependence, and our calculations utilizing def2-SVP are unlikely to be converged; however, the size of the systems considered makes extrapolation to the complete basis set limit infeasible for the purposes of this investigation. **Mn-Nit** again presents an outlier from the experimentally observed ordering of exchange coupling constants in the multireference calculations.

As both DFT and CASSCF successfully recover the experimental ordering of the surveyed compounds in terms of the strength of the exchange interaction, with the minor exception of **Mn-Nit**, the calculated electronic properties should aid with the identification of factors influencing the magnitude of J. Since exchange coupling is a function of the energetic separation of the involved spin states, it should correlate with the degree of multireference character of the wave function of the low-spin ground state. Indeed, direct correlation is observed between the open-shell character of the CASSCF solution as characterized by the natural occupation numbers and the magnitude of spin contamination (or the expectation value of the $\hat{S}^2$ operator) in broken-symmetry DFT, obtained for the $S = 9/2$ ground state (Figure S6).

While these values provide quantum mechanical insight into the origin of the exchange interaction and yield a readily available diagnostic for the in-silico design of systems displaying large J, they provide little insight into the intramolecular interactions that allow for the rational design of such compounds, e.g., via ligand substitution. To this end, further electronic and structural properties were investigated. Prior computational studies have suggested that a shorter bond length between the metal and the radical ligand is correlated with stronger antiferromagnetic coupling.[79−81] Thus, we examined the Mn−linker bond lengths in the crystal structures of **1** and the other complexes displayed in Figure 1. To allow comparison between coordinating atoms of different sizes, we

https://doi.org/10.1021/acs.inorgchem.3c02534
Inorg. Chem. 2023, 62, 19488−19497

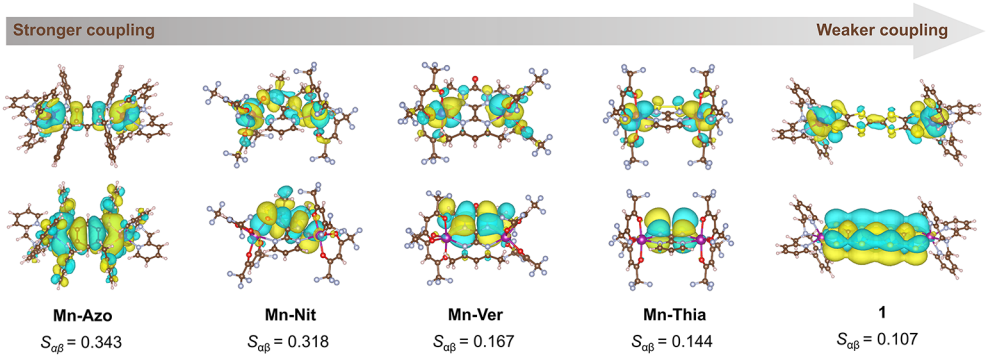

Figure 5. Corresponding orbitals and their overlap integrals ($S_{\alpha\beta}$) for **1** and other Mn(II) complexes derived from BS-DFT orbitals in the $S = 9/2$ ground state.

first normalized the actual bond lengths by the covalent radii of the involved atoms and then calculated their average value (Table S3).[82] For the four complexes reported in the literature, a shorter average Mn−linker bond length indeed reflects a larger magnitude of J as listed in Table 1. However, complex **1**, with relatively short Mn−S bonds, does not match this trend. Repeating this analysis using the bond lengths obtained from DFT optimization still does not fit the trend defined by the other four complexes (Table S4).

Using a series of azophenine radical-bridged complexes as models, a computational study showed that a more covalent metal−nitrogen bond coincided with stronger magnetic coupling.[56,80] Therefore, we computed the Mayer bond orders of the DFT-optimized structures to analyze the effect of bond covalency in the five surveyed Mn complexes (Table S4). Generally, a larger Mn−linker Mayer bond order corresponds to a smaller normalized bond length, and among the four literature examples, **Mn-Azo** with the largest $|J|$ indeed displays the largest Mayer bond orders. However, complex **1** displays an even greater Mn−S covalency despite its small $|J|$. In the studies mentioned above, the identity of the metal species presented the only variable in the series of complexes surveyed, while in this work we examine a variety of radical linkers, resulting in multiple variables affecting the nature of the exchange interaction. Still, our case demonstrates that adopting sulfurs as binding atoms to promote metal−radical bond covalency does not always impart strong magnetic coupling.

We then carried out corresponding orbital transformations using BS-DFT orbitals in the $S = 9/2$ ground state. This analysis generates valence-bond-like magnetic pairs and has been applied successfully to both metal−metal and metal−radical systems to quantify antiferromagnetic coupling.[83−91] The results in Figure 5 show that in each surveyed complex, one magnetic orbital is mainly metal-based, while the orbital with the opposite spin is chiefly ligand-based. In line with other studies, the overlap ($S_{\alpha\beta}$) of the corresponding orbital pair correlates well with the magnitude of J (Table 1 and Figure S7). The large magnitude of $S_{\alpha\beta}$ in **Mn-Azo** is clearly associated with its delocalized character. Four carbons on the ligand are involved in the metal-based orbital, and likewise, two Mn atoms have significant contributions to the ligand-based orbital. Considering the nature of the ligand itself, $TTFtt^{3-\bullet}$ is highly conjugated and delocalized like azophenine.[57] Yet, the metal-based corresponding orbital of **1** is almost entirely localized on the two Mn centers with little contribution from the TTFtt ligand. This results in little overlap or coupling, as illustrated by the small $S_{\alpha\beta}$ value.

Another factor proposed to affect the exchange interaction is the spin density distribution on the radical linker. In studies of radical-bridged dinuclear Fe(II) and Gd(III) complexes, it was shown that in the frontier singly occupied molecular orbitals (SOMOs), larger spin densities on the coordinating atoms of radicals may support stronger metal−radical coupling.[22,24] Hence, we examined the DFT Mulliken spin densities of the $S = 9/2$ state of each complex, summing the spin densities on the coordinating atoms (Tables 1 and S6). In complex **1**, the spin density on the four terminal sulfurs of TTFtt is minimal (0.037), revealing the radical to be mostly localized in the central TTF moiety (Figure 6). By contrast, in the other four complexes, the spin densities on coordinating O and N atoms are significantly larger (>0.51). While CASSCF data differ from DFT in absolute magnitude, spin densities on coordinating atoms in **1** remain 1 order of magnitude lower than those in the other surveyed complexes. In a previous study, we also reported spin density plots of a $TTFtt^{3-\bullet}$-bridged dinuclear Ni(II) complex in the solid state.[57] Though exact numbers were not provided, qualitatively, the spin densities on the coordinating sulfurs are also smaller than those on the central atoms in $TTFtt^{3-\bullet}$. While spin density cannot perfectly rationalize the trend of J across all of the surveyed Mn complexes, **1** indeed shows a distinct spin distribution from the others.

To confirm whether the coordinating sulfur atoms in $TTFtt^{3-\bullet}$ cause any unusual effects to reduce the coupling strength, we performed BS-DFT calculations on a hypothetical complex, **2**, where the four sulfur linkers in **1** are replaced with oxygen. The calculated Mn radical antiferromagnetic coupling in **2** ($J = -5\ cm^{-1}$) is only slightly weaker than that in **1** ($J = -10\ cm^{-1}$). Also, the radical in **2** is again primarily localized on the TTF core, while the sum of spin densities on the oxygen linkers is only 0.072 (Figure S8 and Table S6), which is reminiscent of the pattern in **1**. Therefore, the identity of binding atoms in **1** and **2** does not play a crucial role in magnetic coupling. Overall, the combined computational analyses suggest that isolation between the $TTFtt^{3-\bullet}$ radical electron and the Mn centers in **1** outweighs the potential influence of short, highly covalent Mn−S bonds and diminishes the antiferromagnetic coupling.

These results suggest that other sulfur-based linkers like benzenetetrathiolate (BTT) and other dithiolene radicals, such as those developed by Robinson,[92−94] should be more promising candidates to induce large coupling. DFT calculations suggest appreciable spin densities for the coordinating sulfurs in complexes of these ligands. Indeed,

https://doi.org/10.1021/acs.inorgchem.3c02534
Inorg. Chem. 2023, 62, 19488−19497

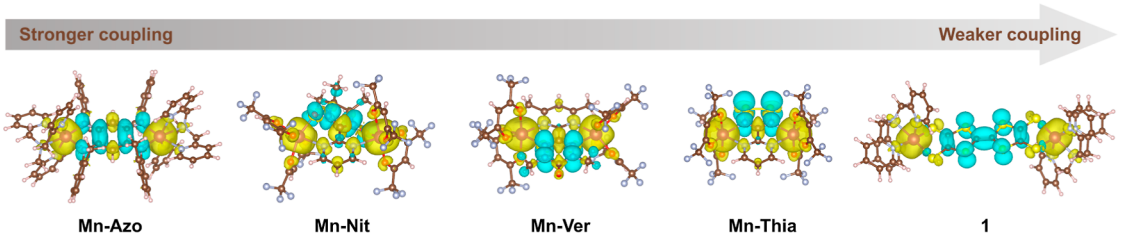

Figure 6. DFT-calculated Mulliken spin density distributions of **1** and other Mn(II) complexes are shown at a 0.0015 isovalue, as obtained at the spin-unrestricted PBE0/def2-TZVP level of theory for the $S = 9/2$ ground state. Cyan and yellow correspond to α and β spin, respectively.

Harris and co-workers already demonstrated large exchange couplings in a Cr(III) complex with $BTT^{3-\bullet}$, albeit with limited thermal stability.[56]

CONCLUSIONS

We report a $TTFtt^{3-\bullet}$-bridged dinuclear Mn(II) complex, which is the first well-characterized species featuring a $TTFtt^{3-\bullet}$ radical bridging paramagnetic metals. Magnetometry measurements reveal that the antiferromagnetic coupling between the radical and metal spins is significantly weaker compared to other Mn−radical compounds previously reported in the literature. DFT computations reveal the weak exchange coupling to be the result of small spatial overlap between the magnetic orbitals, while CASSCF calculations show a high degree of multireference and open-shell character in the $S = 9/2$ solution, leading to small energetic separation between the $S = 9/2$ and $S = 11/2$ states. Additionally, our calculations suggest that the spin density likely plays a more dominant role than metal−linker bond lengths and covalency in determining the exchange interaction of this complex. Here, the $TTFtt^{3-\bullet}$ radical is chiefly localized on the central TTF unit without significant spin density on the terminal coordinating sulfurs. The insights gained in this work provide an important understanding on the electronic structure of the $TTFtt^{3-\bullet}$ radical and also show that multiple competing effects must be considered in the design of radical linkers for molecular magnetic compounds.

EXPERIMENTAL SECTION

General Methods. All reactions and handlings were performed in a MBraun UNIlab glovebox filled with N_2 unless otherwise noted. $TTFtt(CH_2CH_2CN)_4$ and $[Fc^{BzO}][BAr^F{}_4]$ were synthesized following literature procedures.[57,95] $(TPA)MnCl_2$ was synthesized according to a literature procedure except that anhydrous $MnCl_2$ was used instead of the hexahydrate.[96] Anhydrous methanol purchased from Sigma-Aldrich and chlorobenzene (extra dry, AcroSeal) purchased from Thermo Scientific Chemicals were transferred into the glovebox and stored over 4 Å molecular sieves. DCM, petroleum ether, and THF were dried and degassed with N_2 in a Pure Process Technologies solvent system, filtered through alumina, and stored over 4 Å molecular sieves, while THF was stirred over NaK amalgam overnight before filtration. All other reagents were used as purchased from commercial sources without further purification. Elemental analyses were carried out by Midwest Microlabs.

Synthesis of 1 $\{[(TPA)Mn]_2TTFtt\}\{BAr^F{}_4\}$. $TTFtt(CH_2CH_2CN)_4$ (57.3 mg, 0.105 mmol) and sodium *tert*-butoxide (82.0 mg, 0.84 mmol, 8.0 equiv) were stirred in THF (5 mL) overnight. The resulting pink precipitate was separated by centrifugation, washed with THF, and dissolved in methanol. The resulting dark red solution was mixed with a methanolic solution (6 mL) of $(TPA)MnCl_2$ (88.4 mg, 0.21 mmol, 2.0 equiv) and stirred overnight. The resulting red-orange precipitate, presumably $[(TPA)Mn]_2TTFtt$, was separated by centrifugation, washed with methanol, and suspended in DCM (4 mL). A DCM solution (6 mL) of $[Fc^{BzO}][BAr^F{}_4]$ (50.3 mg, 0.044 mmol, 0.4 equiv) was then slowly added into the suspension over 4 h. After stirring overnight, the reaction mixture was filtered through Celite and condensed to 2 mL under reduced pressure. Petroleum ether (10 mL) was then added to precipitate the crude product. The precipitate was dissolved in chlorobenzene/DCM cosolvent (6 mL, 3:2, v/v), and petroleum ether vapor was allowed to diffuse into the solution to yield brown solids. The solids were collected and crystallized again under the same conditions to afford brown single crystals of $\mathbf{1}\cdot 3(C_6H_5Cl)$ suitable for X-ray diffraction analysis. The single crystals were ground to fine powder by a spatula and dried under reduced pressure for 48 h to afford unsolvated complex **1** (45.2 mg, 57% based on $[Fc^{BzO}][BAr^F{}_4]$), which was used for all other characterizations and experiments. ^1H nuclear magnetic resonance (NMR) (500 MHz, CD_2Cl_2, 298 K): δ 7.56 (br s, $[BAr^F{}_4]^-$), 7.73 (br s, $[BAr^F{}_4]^-$). IR (dropcast on KBr plates; cm^{-1}): 2916, 2849, 2687, 1603, 1355, 1276, 1124, 887, 839, 761, 713, 682. Elemental analysis calcd for **1**, $C_{74}H_{48}BF_{24}Mn_2N_8S_8$: C 47.22%, H 2.57%, N 5.95%; found: C 47.65%, H 2.66%, N 6.09%.

In some batches, we noticed the presence of an overoxidized species containing $TTFtt^{2-}$, which showed a distinct NIR absorption at ∼1100 nm.[57−59] To remove this, the product was dissolved in THF (12 mL) as a sacrificial reductant and kept overnight. After removal of THF under reduced pressure, the solid was crystallized by the aforementioned method to afford pure **1**, as confirmed by single-crystal X-ray diffraction (SXRD) and other spectroscopic methods mentioned in this work.

Cyclic Voltammetry. Electrochemical measurements were conducted on a BASi Epsilon potentiostat with a glassy carbon working electrode, a platinum wire counter electrode, and a silver wire pseudoreference electrode. Voltammograms were referenced to internal Fc^+/Fc.

FT-IR Spectroscopy. IR samples were prepared by drop-casting DCM solutions onto KBr plates. Measurements were performed on a Bruker Optics TENSOR II spectrometer with OPUS software. Background subtraction and baseline correction were conducted using OMNIC software.

Magnetometry. Magnetic measurements in the solid state were carried out on a Quantum Design MPMS-XL SQUID. The powder samples were suspended in an eicosane matrix inside polycarbonate capsules. The χT vs temperature data were fitted with program PHI.[68] Pascal's constants were adopted to correct for the diamagnetic contribution from the complex.[97]

Nuclear Magnetic Resonance. ^1H NMR spectra were collected on a Bruker Avance II+ 500 MHz spectrometer, and chemical shifts (δ) were reported in parts per million (ppm) with CD_2Cl_2 ($\delta = 5.32$) as the internal standard. Evans' method was conducted in CD_2Cl_2/CH_2Cl_2 (50:1, v/v) with a capillary insert containing the same solvent. Pascal's constants were adopted to correct for the diamagnetic contribution from the complex.[97]

Single-Crystal X-ray Diffraction. SXRD data were collected at 100 K on a Bruker D8 Venture diffractometer with a PHOTON 100 CMOS detector and a Mo-target microfocus X-ray tube ($\lambda = 0.71073$ Å). Data reduction and integration were performed with the Bruker APEX3 software package (Bruker AXS, version 2015.5−2, 2015).[98] Data were scaled and corrected for absorption effects using the multiscan procedure as implemented in SADABS (Bruker AXS,

https://doi.org/10.1021/acs.inorgchem.3c02534
Inorg. Chem. 2023, 62, 19488−19497

version 2014/54, 2015). Crystal structures were solved by SHELXT (version 2014/55) and refined by a full-matrix least-squares procedure using OLEX26 (XL refinement program version 2018/17).[99,100]

UV−Vis−NIR. UV−vis−NIR spectra were recorded on a Shimadzu UV-3600 Plus spectrophotometer.

■ ASSOCIATED CONTENT

Supporting Information

The Supporting Information is available free of charge at https://pubs.acs.org/doi/10.1021/acs.inorgchem.3c02534.

NMR and IR spectra, crystallographic data, and detailed computational results (PDF)

Accession Codes

CCDC 2256615 contains the supplementary crystallographic data for this paper. These data can be obtained free of charge via www.ccdc.cam.ac.uk/data_request/cif, by emailing to data_request@ccdc.cam.ac.uk, or by contacting The Cambridge Crystallographic Data Centre, 12 Union Road, Cambridge CB2 1EZ, UK; fax: +44 1223 336033.

■ AUTHOR INFORMATION

Corresponding Author

John S. Anderson − *Department of Chemistry, University of Chicago, Chicago, Illinois 60637, United States;* orcid.org/0000-0002-0730-3018; Email: jsanderson@uchicago.edu

Authors

Chen-Yu Lien − *Department of Chemistry, University of Chicago, Chicago, Illinois 60637, United States*

Jan-Niklas Boyn − *Department of Mechanical and Aerospace Engineering, Princeton University, Princeton, New Jersey 08544, United States*

Sophie W. Anferov − *Department of Chemistry, University of Chicago, Chicago, Illinois 60637, United States;* orcid.org/0000-0003-3972-5845

David A. Mazziotti − *Department of Chemistry, University of Chicago, Chicago, Illinois 60637, United States;* orcid.org/0000-0002-9938-3886

Complete contact information is available at: https://pubs.acs.org/10.1021/acs.inorgchem.3c02534

Notes

The authors declare no competing financial interest.

■ ACKNOWLEDGMENTS

J.S.A. gratefully acknowledges support for this work from the United States Army Research Office (ARO) grant no. W911NF-23-1-0233. J.S.A. and D.A.M. gratefully acknowledge support for this work from the U.S. Department of Energy, Office of Science, Office of Basic Energy Sciences, under the grant DE-SC0019215. D.A.M. also acknowledges support for this work from the National Science Foundation under award number CHE-2155082. This work made use of the shared facilities at the University of Chicago Materials Research Science and Engineering Center, supported by the National Science Foundation under award number DMR-2011854. J.S.A. also gratefully acknowledges support from the Dreyfus Foundation for a Teacher-Scholar Award (TC-21-064). Parts of this work were carried out at the Soft Matter Characterization Facility of the University of Chicago.

■ REFERENCES

(1) Thorarinsdottir, A. E.; Harris, T. D. Metal-Organic Framework Magnets. *Chem. Rev.* **2020**, *120*, 8716−8789.

(2) Demir, S.; Jeon, I.-R.; Long, J. R.; Harris, T. D. Radical ligand-containing single-molecule magnets. *Coord. Chem. Rev.* **2015**, *289*−*290*, 149−176.

(3) Zabala-Lekuona, A.; Seco, J. M.; Colacio, E. Single-Molecule Magnets: From Mn12-ac to dysprosium metallocenes, a travel in time. *Coord. Chem. Rev.* **2021**, *441*, 213984.

(4) Zhang, P.; Guo, Y.-N.; Tang, J. Recent advances in dysprosium-based single molecule magnets: Structural overview and synthetic strategies. *Coord. Chem. Rev.* **2013**, *257*, 1728−1763.

(5) Murrie, M. Cobalt(ii) single-molecule magnets. *Chem. Soc. Rev.* **2010**, *39*, 1986−1995.

(6) Zheng, Y.-Z.; Zhou, G.-J.; Zheng, Z.; Winpenny, R. E. P. Molecule-based magnetic coolers. *Chem. Soc. Rev.* **2014**, *43*, 1462−1475.

(7) Miller, J. S. Magnetically ordered molecule-based materials. *Chem. Soc. Rev.* **2011**, *40*, 3266−3296.

(8) Verdaguer, M.; Bleuzen, A.; Marvaud, V.; Vaissermann, J.; Seuleiman, M.; Desplanches, C.; Scuiller, A.; Train, C.; Garde, R.; Gelly, G.; Lomenech, C.; Rosenman, I.; Veillet, P.; Cartier, C.; Villain, F. Molecules to build solids: high T_C molecule-based magnets by design and recent revival of cyano complexes chemistry. *Coord. Chem. Rev.* **1999**, *190*−*192*, 1023−1047.

(9) Wang, X.-Y.; Avendaño, C.; Dunbar, K. R. Molecular magnetic materials based on 4d and 5d transition metals. *Chem. Soc. Rev.* **2011**, *40*, 3213−3238.

(10) Woodruff, D. N.; Winpenny, R. E. P.; Layfield, R. A. Lanthanide Single-Molecule Magnets. *Chem. Rev.* **2013**, *113*, 5110−5148.

(11) Freedman, D. E.; Jenkins, D. M.; Iavarone, A. T.; Long, J. R. A Redox-Switchable Single-Molecule Magnet Incorporating $[Re(CN)_7]_3$. *J. Am. Chem. Soc.* **2008**, *130*, 2884−2885.

(12) Fortier, S.; Le Roy, J. J.; Chen, C.-H.; Vieru, V.; Murugesu, M.; Chibotaru, L. F.; Mindiola, D. J.; Caulton, K. G. A Dinuclear Cobalt Complex Featuring Unprecedented Anodic and Cathodic Redox Switches for Single-Molecule Magnet Activity. *J. Am. Chem. Soc.* **2013**, *135*, 14670−14678.

(13) Ma, X.; Suturina, E. A.; De, S.; Négrier, P.; Rouzières, M.; Clérac, R.; Dechambenoit, P. A Redox-Active Bridging Ligand to Promote Spin Delocalization, High-Spin Complexes, and Magnetic Multi-Switchability. *Angew. Chem., Int. Ed.* **2018**, *57*, 7841−7845.

(14) Liu, L.; DeGayner, J. A.; Sun, L.; Zee, D. Z.; Harris, T. D. Reversible redox switching of magnetic order and electrical conductivity in a 2D manganese benzoquinoid framework. *Chem. Sci.* **2019**, *10*, 4652−4661.

(15) Gütlich, P.; Hauser, A. Thermal and light-induced spin crossover in iron(II) complexes. *Coord. Chem. Rev.* **1990**, *97*, 1−22.

(16) Hauser, A. Light-Induced Spin Crossover and the High-Spin→Low-Spin Relaxation. *Spin Crossover in Transition Metal Compounds II*; Springer Berlin Heidelberg: Berlin, Heidelberg, 2004; pp 155−198.

(17) Nakaya, M.; Ohtani, R.; Lindoy, L. F.; Hayami, S. Light-induced excited spin state trapping in iron(iii) complexes. *Inorg. Chem. Front.* **2021**, *8*, 484−498.

(18) Milon, J.; Daniel, M.-C.; Kaiba, A.; Guionneau, P.; Brandès, S.; Sutter, J.-P. Nanoporous Magnets of Chiral and Racemic $[\{Mn(HL)\}_2Mn\{Mo(CN)_7\}_2]$ with Switchable Ordering Temperatures (T_C = 85 K ↔ 106 K) Driven by H_2O Sorption (L = N,N-Dimethylalaninol). *J. Am. Chem. Soc.* **2007**, *129*, 13872−13878.

(19) Shao, D.; Shi, L.; Yin, L.; Wang, B.-L.; Wang, Z.-X.; Zhang, Y.-Q.; Wang, X.-Y. Reversible on-off switching of both spin crossover and single-molecule magnet behaviours via a crystal-to-crystal transformation. *Chem. Sci.* **2018**, *9*, 7986−7991.

(20) Zhang, J.; Kosaka, W.; Sugimoto, K.; Miyasaka, H. Magnetic Sponge Behavior via Electronic State Modulations. *J. Am. Chem. Soc.* **2018**, *140*, 5644−5652.

(21) Huang, Y.; Zhang, Q.; Li, Y. C.; Yao, Y.; Hu, Y.; Ren, S. Chemical Tuning Meets 2D Molecular Magnets. *Adv. Mater.* **2023**, *35*, 2208919.
(22) Gould, C. A.; Mu, E.; Vieru, V.; Darago, L. E.; Chakarawet, K.; Gonzalez, M. I.; Demir, S.; Long, J. R. Substituent Effects on Exchange Coupling and Magnetic Relaxation in 2,2'-Bipyrimidine Radical-Bridged Dilanthanide Complexes. *J. Am. Chem. Soc.* **2020**, *142*, 21197−21209.
(23) Liu, S.-S.; Xu, L.; Jiang, S.-D.; Zhang, Y.-Q.; Meng, Y.-S.; Wang, Z.; Wang, B.-W.; Zhang, W.-X.; Xi, Z.; Gao, S. Half-Sandwich Complexes of Dy^{III}: A Janus-Motif with Facile Tunability of Magnetism. *Inorg. Chem.* **2015**, *54*, 5162−5168.
(24) Thorarinsdottir, A. E.; Bjornsson, R.; Harris, T. D. Insensitivity of Magnetic Coupling to Ligand Substitution in a Series of Tetraoxolene Radical-Bridged Fe_2 Complexes. *Inorg. Chem.* **2020**, *59*, 4634−4649.
(25) Sato, O.; Tao, J.; Zhang, Y.-Z. Control of Magnetic Properties through External Stimuli. *Angew. Chem., Int. Ed.* **2007**, *46*, 2152−2187.
(26) Lannes, A.; Suffren, Y.; Tommasino, J. B.; Chiriac, R.; Toche, F.; Khrouz, L.; Molton, F.; Duboc, C.; Kieffer, I.; Hazemann, J.-L.; Reber, C.; Hauser, A.; Luneau, D. Room Temperature Magnetic Switchability Assisted by Hysteretic Valence Tautomerism in a Layered Two-Dimensional Manganese-Radical Coordination Framework. *J. Am. Chem. Soc.* **2016**, *138*, 16493−16501.
(27) Urtizberea, A.; Roubeau, O. Switchable slow relaxation of magnetization in the native low temperature phase of a cooperative spin-crossover compound. *Chem. Sci.* **2017**, *8*, 2290−2295.
(28) Mitsumi, M.; Nishitani, T.; Yamasaki, S.; Shimada, N.; Komatsu, Y.; Toriumi, K.; Kitagawa, Y.; Okumura, M.; Miyazaki, Y.; Górska, N.; Inaba, A.; Kanda, A.; Hanasaki, N. Bistable Multifunctionality and Switchable Strong Ferromagnetic-to-Antiferromagnetic Coupling in a One-Dimensional Rhodium(I)-Semiquinonato Complex. *J. Am. Chem. Soc.* **2014**, *136*, 7026−7037.
(29) Henkelis, S. E.; Huber, D. L.; Vogel, D. J.; Rimsza, J. M.; Nenoff, T. M. Magnetic Tunability in RE-DOBDC MOFs via NOx Acid Gas Adsorption. *ACS Appl. Mater. Interfaces* **2020**, *12*, 19504−19510.
(30) Pointillart, F.; le Guennic, B.; Cador, O.; Maury, O.; Ouahab, L. Lanthanide Ion and Tetrathiafulvalene-Based Ligand as a "Magic" Couple toward Luminescence, Single Molecule Magnets, and Magnetostructural Correlations. *Acc. Chem. Res.* **2015**, *48*, 2834−2842.
(31) Long, J.; Guari, Y.; Ferreira, R. A. S.; Carlos, L. D.; Larionova, J. Recent advances in luminescent lanthanide based Single-Molecule Magnets. *Coord. Chem. Rev.* **2018**, *363*, 57−70.
(32) Jiang, X.; Liu, Q.; Xing, J.; Liu, N.; Guo, Y.; Liu, Z.; Zhao, J. Recent progress on 2D magnets: Fundamental mechanism, structural design and modification. *Appl. Phys. Rev.* **2021**, *8*, 031305.
(33) Frecus, B.; Oprea, C. I.; Panait, P.; Ferbinteanu, M.; Cimpoesu, F.; Gîrţu, M. A. Ab initio study of exchange coupling for the consistent understanding of the magnetic ordering at room temperature in $V[TCNE]_x$. *Theor. Chem. Acc.* **2014**, *133*, 1470.
(34) Ashcroft, N. W.; Mermin, N. D. *Solid State Physics*; Saunders College: Philadelphia, 1976.
(35) Langley, S. K.; Wielechowski, D. P.; Vieru, V.; Chilton, N. F.; Moubaraki, B.; Abrahams, B. F.; Chibotaru, L. F.; Murray, K. S. A $\{Cr^{III}_2Dy^{III}_2\}$ Single-Molecule Magnet: Enhancing the Blocking Temperature through 3d Magnetic Exchange. *Angew. Chem., Int. Ed.* **2013**, *52*, 12014−12019.
(36) Vignesh, K. R.; Langley, S. K.; Murray, K. S.; Rajaraman, G. Quenching the Quantum Tunneling of Magnetization in Heterometallic Octanuclear $\{TM^{III}_4Dy^{III}_4\}$ (TM = Co and Cr) Single-Molecule Magnets by Modification of the Bridging Ligands and Enhancing the Magnetic Exchange Coupling. *Chem.—Eur. J.* **2017**, *23*, 1654−1666.
(37) Swain, A.; Sharma, T.; Rajaraman, G. Strategies to quench quantum tunneling of magnetization in lanthanide single molecule magnets. *Chem. Commun.* **2023**, *59*, 3206−3228.
(38) Wang, X.-Y.; Wang, Z.-M.; Gao, S. Constructing magnetic molecular solids by employing three-atom ligands as bridges. *Chem. Commun.* **2008**, 281−294.
(39) Dechambenoit, P.; Long, J. R. Microporous magnets. *Chem. Soc. Rev.* **2011**, *40*, 3249−3265.
(40) Boyn, J.-N.; Xie, J.; Anderson, J. S.; Mazziotti, D. A. Entangled Electrons Drive a Non-superexchange Mechanism in a Cobalt Quinoid Dimer Complex. *J. Phys. Chem. Lett.* **2020**, *11*, 4584−4590.
(41) Sessoli, R.; Tsai, H. L.; Schake, A. R.; Wang, S.; Vincent, J. B.; Folting, K.; Gatteschi, D.; Christou, G.; Hendrickson, D. N. High-spin molecules: $[Mn_{12}O_{12}(O_2CR)_{16}(H_2O)_4]$. *J. Am. Chem. Soc.* **1993**, *115*, 1804−1816.
(42) Das, V.; Kaushik, R.; Hussain, F. Heterometallic 3d-4f polyoxometalates: An emerging field with structural diversity to multiple applications. *Coord. Chem. Rev.* **2020**, *413*, 213271.
(43) Clemente-Juan, J. M.; Coronado, E.; Gaita-Ariño, A. Magnetic polyoxometalates: from molecular magnetism to molecular spintronics and quantum computing. *Chem. Soc. Rev.* **2012**, *41*, 7464−7478.
(44) Gatteschi, D.; Caneschi, A.; Pardi, L.; Sessoli, R. Large Clusters of Metal Ions: The Transition from Molecular to Bulk Magnets. *Science* **1994**, *265*, 1054−1058.
(45) Ferlay, S.; Mallah, T.; Ouahès, R.; Veillet, P.; Verdaguer, M. A room-temperature organometallic magnet based on Prussian blue. *Nature* **1995**, *378*, 701−703.
(46) Cernák, J.; Orendáč, M.; Potočňák, I.; Chomič, J.; Orendáčová, A.; Skoršepa, J.; Feher, A. Cyanocomplexes with one-dimensional structures: preparations, crystal structures and magnetic properties. *Coord. Chem. Rev.* **2002**, *224*, 51−66.
(47) Kurmoo, M. Magnetic metal-organic frameworks. *Chem. Soc. Rev.* **2009**, *38*, 1353−1379.
(48) Habib, F.; Murugesu, M. Lessons learned from dinuclear lanthanide nano-magnets. *Chem. Soc. Rev.* **2013**, *42*, 3278−3288.
(49) Caneschi, A.; Gatteschi, D.; Sessoli, R.; Rey, P. Toward molecular magnets: the metal-radical approach. *Acc. Chem. Res.* **1989**, *22*, 392−398.
(50) Jeon, I.-R.; Park, J. G.; Xiao, D. J.; Harris, T. D. An Azophenine Radical-Bridged Fe_2 Single-Molecule Magnet with Record Magnetic Exchange Coupling. *J. Am. Chem. Soc.* **2013**, *135*, 16845−16848.
(51) Pedersen, K. S.; Perlepe, P.; Aubrey, M. L.; Woodruff, D. N.; Reyes-Lillo, S. E.; Reinholdt, A.; Voigt, L.; Li, Z.; Borup, K.; Rouzières, M.; Samohvalov, D.; Wilhelm, F.; Rogalev, A.; Neaton, J. B.; Long, J. R.; Clérac, R. Formation of the layered conductive magnet $CrCl_2(pyrazine)_2$ through redox-active coordination chemistry. *Nat. Chem.* **2018**, *10*, 1056−1061.
(52) DeGayner, J. A.; Jeon, I.-R.; Harris, T. D. A series of tetraazalene radical-bridged M_2 ($M = Cr^{III}$, Mn^{II}, Fe^{II}, Co^{II}) complexes with strong magnetic exchange coupling. *Chem. Sci.* **2015**, *6*, 6639−6648.
(53) Wu, J.; MacDonald, D. J.; Clérac, R.; Jeon, I.-R.; Jennings, M.; Lough, A. J.; Britten, J.; Robertson, C.; Dube, P. A.; Preuss, K. E. Metal Complexes of Bridging Neutral Radical Ligands: pymDTDA and pymDSDA. *Inorg. Chem.* **2012**, *51*, 3827−3839.
(54) Barclay, T. M.; Hicks, R. G.; Lemaire, M. T.; Thompson, L. K. Synthesis, Structure, and Magnetism of Bimetallic Manganese or Nickel Complexes of a Bridging Verdazyl Radical. *Inorg. Chem.* **2001**, *40*, 5581−5584.
(55) Miao, H.; Li, M.; Li, H.-Q.; Shen, F.-X.; Zhang, Y.-Q.; Wang, X.-Y. Syntheses and magnetic properties of a bis-tridentate nitronyl nitroxide radical and its metal complexes. *Dalton Trans.* **2019**, *48*, 4774−4778.
(56) Hua, C.; DeGayner, J. A.; Harris, T. D. Thiosemiquinoid Radical-Bridged Cr^{III}_2 Complexes with Strong Magnetic Exchange Coupling. *Inorg. Chem.* **2019**, *58*, 7044−7053.
(57) Xie, J.; Boyn, J.-N.; Filatov, A. S.; McNeece, A. J.; Mazziotti, D. A.; Anderson, J. S. Redox, transmetalation, and stacking properties of tetrathiafulvalene-2,3,6,7-tetrathiolate bridged tin, nickel, and palladium compounds. *Chem. Sci.* **2020**, *11*, 1066−1078.

https://doi.org/10.1021/acs.inorgchem.3c02534
Inorg. Chem. 2023, 62, 19488−19497

(58) Kawamura, A.; Xie, J.; Boyn, J.-N.; Jesse, K. A.; McNeece, A. J.; Hill, E. A.; Collins, K. A.; Valdez-Moreira, J. A.; Filatov, A. S.; Kurutz, J. W.; Mazziotti, D. A.; Anderson, J. S. Reversible Switching of Organic Diradical Character via Iron-Based Spin-Crossover. *J. Am. Chem. Soc.* **2020**, *142*, 17670−17680.
(59) McNamara, L. E.; Boyn, J.-N.; Melnychuk, C.; Anferov, S. W.; Mazziotti, D. A.; Schaller, R. D.; Anderson, J. S. Bright, Modular, and Switchable Near-Infrared II Emission from Compact Tetrathiafulvalene-Based Diradicaloid Complexes. *J. Am. Chem. Soc.* **2022**, *144*, 16447−16455.
(60) Xie, J.; Ewing, S.; Boyn, J.-N.; Filatov, A. S.; Cheng, B.; Ma, T.; Grocke, G. L.; Zhao, N.; Itani, R.; Sun, X.; Cho, H.; Chen, Z.; Chapman, K. W.; Patel, S. N.; Talapin, D. V.; Park, J.; Mazziotti, D. A.; Anderson, J. S. Intrinsic glassy-metallic transport in an amorphous coordination polymer. *Nature* **2022**, *611*, 479−484.
(61) Xie, J.; Pan, J.-A.; Cheng, B.; Ma, T.; Filatov, A. S.; Patel, S. N.; Park, J.; Talapin, D. V.; Anderson, J. S. Presynthetic Redox Gated Metal-to-Insulator Transition and Photothermoelectric Properties in Nickel Tetrathiafulvalene-Tetrathiolate Coordination Polymers. *J. Am. Chem. Soc.* **2022**, *144*, 19026−19037.
(62) Roos, B. O. The Complete Active Space Self-Consistent Field Method and its Applications in Electronic Structure Calculations. *Adv. Chem. Phys.* **1987**, *69*, 399−445.
(63) Ruiz, E.; Cano, J.; Alvarez, S.; Alemany, P. Broken symmetry approach to calculation of exchange coupling constants for homobinuclear and heterobinuclear transition metal complexes. *J. Comput. Chem.* **1999**, *20*, 1391−1400.
(64) Lin, C.-H.; Chen, C.-G.; Tsai, M.-L.; Lee, G.-H.; Liaw, W.-F. Monoanionic $\{Mn(NO)\}^5$ and Dianionic $\{Mn(NO)\}^6$ Thiolatonitrosylmanganese Complexes: $[(NO)\ Mn(L)_2]^-$ and $[(NO)\ Mn(L)_2]^{2-}$ (LH_2 = 1,2-Benzenedithiol and Toluene-3,4-dithiol). *Inorg. Chem.* **2008**, *47*, 11435−11443.
(65) Heinl, U.; Kleinitz, U.; Mattes, R. Koordinationspolymere 1, 2-Dithiooxalato- und 1, 2-Dithioquadratato-Komplexe. Synthese und Strukturen von $[BaCr_2(bipy)_2(1, 2\text{-dtox})_4(H_2O)_2]$, [Ni(cyclam)(1, 2-dtsq)]·2DMF, [Ni(cyclam) Mn(1, 2-dtsq)$_2$$(H_2O)_2$]·2$H_2O$ und $[H_3O]\ [H_5O_2]\ [Cu(cyclam)]_3[Cu_2(1, 2\text{-dtsq})_3]_2$. *Z. Anorg. Allg. Chem.* **2002**, *628*, 2409−2414.
(66) Tamura, H.; Tanaka, S.; Matsubayashi, G.-e.; Mori, W. Crystal structure and magnetic properties of $[NMe_4]_4[Mn_2(C_3S_5)_4]$ ($C_3S_5^{2-}$ = 4,5-dimercaptoc-1,3-dithiole-2-thionate). *Inorg. Chim. Acta* **1995**, *232*, 51−55.
(67) Min, K. S.; DiPasquale, A. G.; Golen, J. A.; Rheingold, A. L.; Miller, J. S. Synthesis, Structure, and Magnetic Properties of Valence Ambiguous Dinuclear Antiferromagnetically Coupled Cobalt and Ferromagnetically Coupled Iron Complexes Containing the Chloranilate(2-) and the Significantly Stronger Coupling Chloranilate(•3-) Radical Trianion. *J. Am. Chem. Soc.* **2007**, *129*, 2360−2368.
(68) Chilton, N. F.; Anderson, R. P.; Turner, L. D.; Soncini, A.; Murray, K. S. PHI: A powerful new program for the analysis of anisotropic monomeric and exchange-coupled polynuclear d- and f-block complexes. *J. Comput. Chem.* **2013**, *34*, 1164−1175.
(69) Luneau, D.; Risoan, G.; Rey, P.; Grand, A.; Caneschi, A.; Gatteschi, D.; Laugier, J. Transition metal derivatives of a chelating nitronyl nitroxide ligand. Nickel(II) and manganese(II) complexes. *Inorg. Chem.* **1993**, *32*, 5616−5622.
(70) Hicks, R. G.; Lemaire, M. T.; Thompson, L. K.; Barclay, T. M. Strong Ferromagnetic and Antiferromagnetic Exchange Coupling between Transition Metals and Coordinated Verdazyl Radicals. *J. Am. Chem. Soc.* **2000**, *122*, 8077−8078.
(71) Angeli, C.; Cimiraglia, R.; Evangelisti, S.; Leininger, T.; Malrieu, J.-P. Introduction of n-electron valence states for multireference perturbation theory. *J. Chem. Phys.* **2001**, *114*, 10252−10264.
(72) Weigend, F.; Ahlrichs, R. Balanced basis sets of split valence, triple zeta valence and quadruple zeta valence quality for H to Rn: Design and assessment of accuracy. *Phys. Chem. Chem. Phys.* **2005**, *7*, 3297−3305.
(73) Adamo, C.; Barone, V. Toward reliable density functional methods without adjustable parameters: The PBE0 model. *J. Chem. Phys.* **1999**, *110*, 6158−6170.
(74) Frisch, M. J.; Trucks, G. W.; Schlegel, H. B.; Scuseria, G. E.; Robb, M. A.; Cheeseman, J. R.; Scalmani, G.; Barone, V.; Petersson, G. A.; Nakatsuji, H.; Li, X.; Caricato, M.; Marenich, A. V.; Bloino, J.; Janesko, B. G.; Gomperts, R.; Mennucci, B.; Hratchian, H. P.; Ortiz, J. V.; Izmaylov, A. F.; Sonnenberg, J. L.; Williams; Ding, F.; Lipparini, F.; Egidi, F.; Goings, J.; Peng, B.; Petrone, A.; Henderson, T.; Ranasinghe, D.; Zakrzewski, V. G.; Gao, J.; Rega, N.; Zheng, G.; Liang, W.; Hada, M.; Ehara, M.; Toyota, K.; Fukuda, R.; Hasegawa, J.; Ishida, M.; Nakajima, T.; Honda, Y.; Kitao, O.; Nakai, H.; Vreven, T.; Throssell, K.; Montgomery, J. A.; Peralta, J. E.; Ogliaro, F.; Bearpark, M. J.; Heyd, J. J.; Brothers, E. N.; Kudin, K. N.; Staroverov, V. N.; Keith, T. A.; Kobayashi, R.; Normand, J.; Raghavachari, K.; Rendell, A. P.; Burant, J. C.; Iyengar, S. S.; Tomasi, J.; Cossi, M.; Millam, J. M.; Klene, M.; Adamo, C.; Cammi, R.; Ochterski, J. W.; Martin, R. L.; Morokuma, K.; Farkas, O.; Foresman, J. B.; Fox, D. J. *Gaussian 16*, Revision C.01; Gaussian, Inc.: Wallingford, CT, 2016.
(75) Neese, F.; Wennmohs, F.; Becker, U.; Riplinger, C. The ORCA quantum chemistry program package. *J. Chem. Phys.* **2020**, *152*, 224108.
(76) Weigend, F. Hartree-Fock exchange fitting basis sets for H to Rn †. *J. Comput. Chem.* **2008**, *29*, 167−175.
(77) Soda, T.; Kitagawa, Y.; Onishi, T.; Takano, Y.; Shigeta, Y.; Nagao, H.; Yoshioka, Y.; Yamaguchi, K. Ab initio computations of effective exchange integrals for H-H, H-He-H and Mn_2O_2 complex: comparison of broken-symmetry approaches. *Chem. Phys. Lett.* **2000**, *319*, 223−230.
(78) Llunell, M.; Casanova, D.; Cirera, J.; Alemany, P.; Alvarez, S. *SHAPE. Program for the Stereochemical Analysis of Molecular Fragments by Means of Continuous Shape Measures and Associated Tools*; Universitat de Barcelona: Barcelona, 2013. accessed 2023−09−29. https://www.ee.ub.edu/download/1394/?tmstv=1697137058.
(79) Wei, H.; Wang, F.; Chen, Z. A density functional study on magnetic exchange interaction between Mn(II) ion and nitronyl nitroxide radical in trans-and cis-metal-radical complexes. *Sci. China, Ser. B: Chem.* **2005**, *48*, 402−414.
(80) Singh, M. K. Probing the strong magnetic exchange behaviour of transition metal-radical complexes: a DFT case study. *Dalton Trans.* **2020**, *49*, 4539−4548.
(81) Gupta, T.; Rajeshkumar, T.; Rajaraman, G. Magnetic exchange in $\{Gd^{III}$-radical$\}$ complexes: method assessment, mechanism of coupling and magneto-structural correlations. *Phys. Chem. Chem. Phys.* **2014**, *16*, 14568−14577.
(82) Cordero, B.; Gómez, V.; Platero-Prats, A. E.; Revés, M.; Echeverría, J.; Cremades, E.; Barragán, F.; Alvarez, S. Covalent radii revisited. *Dalton Trans.* **2008**, 2832−2838.
(83) Amos, A. T.; Hall, G. G.; Jones, H. Single determinant wave functions. *Proc. R. Soc. London, Ser. A* **1961**, *263*, 483−493.
(84) Neese, F. Definition of corresponding orbitals and the diradical character in broken symmetry DFT calculations on spin coupled systems. *J. Phys. Chem. Solids* **2004**, *65*, 781−785.
(85) Blanchard, S.; Neese, F.; Bothe, E.; Bill, E.; Weyhermüller, T.; Wieghardt, K. Square Planar vs Tetrahedral Coordination in Diamagnetic Complexes of Nickel(II) Containing Two Bidentate π-Radical Monoanions. *Inorg. Chem.* **2005**, *44*, 3636−3656.
(86) Muresan, N.; Lu, C. C.; Ghosh, M.; Peters, J. C.; Abe, M.; Henling, L. M.; Weyhermöller, T.; Bill, E.; Wieghardt, K. Bis(α-diimine)iron Complexes: Electronic Structure Determination by Spectroscopy and Broken Symmetry Density Functional Theoretical Calculations. *Inorg. Chem.* **2008**, *47*, 4579−4590.
(87) Ye, S.; Tuttle, T.; Bill, E.; Simkhovich, L.; Gross, Z.; Thiel, W.; Neese, F. The Electronic Structure of Iron Corroles: A Combined Experimental and Quantum Chemical Study. *Chem.—Eur. J.* **2008**, *14*, 10839−10851.
(88) Vélez, E.; Alberola, A.; Polo, V. A Density Functional Theory Study of the Magnetic Exchange Coupling in Dinuclear Manganese-

(II) Inverse Crown Structures. *J. Phys. Chem. A* **2009**, *113*, 14008−14013.
(89) Pantazis, D. A.; Krewald, V.; Orio, M.; Neese, F. Theoretical magnetochemistry of dinuclear manganese complexes: broken symmetry density functional theory investigation on the influence of bridging motifs on structure and magnetism. *Dalton Trans.* **2010**, *39*, 4959−4967.
(90) Pantazis, D. A. Meeting the Challenge of Magnetic Coupling in a Triply-Bridged Chromium Dimer: Complementary Broken-Symmetry Density Functional Theory and Multireference Density Matrix Renormalization Group Perspectives. *J. Chem. Theory Comput.* **2019**, *15*, 938−948.
(91) Roy, S.; Paul, S.; Misra, A. A Theoretical Account of the Coupling between Metal- and Ligand-centred Spins. *ChemPhysChem* **2023**, *24*, No. e202200889.
(92) Wang, Y.; Hickox, H. P.; Xie, Y.; Wei, P.; Blair, S. A.; Johnson, M. K.; Schaefer, H. F.; Robinson, G. H. A Stable Anionic Dithiolene Radical. *J. Am. Chem. Soc.* **2017**, *139*, 6859−6862.
(93) Youssef, K.; Poidevin, C.; Vacher, A.; Gal, Y. L.; Charpentier, O.; Fourmigué, M.; Fihey, A.; Barrière, F.; Roisnel, T.; Lorcy, D. A Bimetallic Benzene-1,2,4,5-Tetrathiolate (btt) Molybdenocene Complex $Cp_2Mo(btt)MoCp_2$: Radical and Diradical States. *Chem.—Eur. J.* **2023**, *29*, No. e202300584.
(94) Wang, Y.; Xie, Y.; Wei, P.; Blair, S. A.; Cui, D.; Johnson, M. K.; Schaefer, H. F.; Robinson, G. H. Stable Boron Dithiolene Radicals. *Angew. Chem., Int. Ed.* **2018**, *57*, 7865−7868.
(95) Svenstrup, N.; Rasmussen, K. M.; Hansen, T. K.; Becher, J. The Chemistry of TTFTT; 1: New Efficient Synthesis and Reactions of Tetrathiafulvalene-2,3,6,7-tetrathiolate (TTFTT): An Important Building Block in TTF-Syntheses. *Synthesis* **1994**, *1994*, 809−812.
(96) Hitomi, Y.; Ando, A.; Matsui, H.; Ito, T.; Tanaka, T.; Ogo, S.; Funabiki, T. Aerobic Catechol Oxidation Catalyzed by a Bis(μ-oxo) dimanganese(III,III) Complex via a Manganese(II)-Semiquinonate Complex. *Inorg. Chem.* **2005**, *44*, 3473−3478.
(97) Bain, G. A.; Berry, J. F. Diamagnetic Corrections and Pascal's Constants. *J. Chem. Educ.* **2008**, *85*, 532.
(98) Sheldrick, G. M. Crystal structure refinement with SHELXL. *Acta Crystallogr., Sect. C: Struct. Chem.* **2015**, *71*, 3−8.
(99) Dolomanov, O. V.; Bourhis, L. J.; Gildea, R. J.; Howard, J. A. K.; Puschmann, H. OLEX2: a complete structure solution, refinement and analysis program. *J. Appl. Crystallogr.* **2009**, *42*, 339−341.
(100) Sheldrick, G. M. SHELXT - Integrated space-group and crystal-structure determination. *Acta Crystallogr., Sect. A* **2015**, *71*, 3−8.

https://doi.org/10.1021/acs.inorgchem.3c02534
Inorg. Chem. 2023, 62, 19488−19497